

Impact of Interference on OFDM based Radars

H.C. Yildirim^{*1}, J. Louveaux^{†2}, P. De Doncker^{*3} and F. Horlin^{*4}

^{*}Université Libre de Bruxelles - [†]Université Catholique de Louvain

Email: {¹hayildir, ³pdedonck, ⁴fhorlin}@ulb.ac.be, ²jerome.louveaux@uclouvain.be

Abstract—The goal of this work is to identify the possible degradations on a Wi-Fi based Passive Radar in the presence of an interferer. We assume that the signal-of-opportunity and the interference are 802.11ax compliant. The mathematical model derived for the interference shows that in a synchronized case, the interference may yield ghost targets. When a more occasional interference scenario is considered, the range/Doppler Map accuracy decreases significantly. Furthermore, numerical results are provided to quantify certain effects of OFDM radar interference on range/Doppler Maps.

Index Terms—Passive radar, OFDM radar, 802.11ax, radar interference

I. INTRODUCTION

Passive Radars (PR) are devices that use the signals transmitted by non-cooperative sources as signal-of-opportunity (SoO) in order to estimate channel parameters. From a PR point-of-view, the emerging Wi-Fi standard, 802.11ax [1], or simply 11ax, provides sufficient accuracy for range estimation due to wider bandwidths available at 5 GHz [2]. The goal of each 802.11 amendment is to increase the throughput while maintaining or improving the reliability of the communication. The 11ax takes a step forward and aims to cover a wider range of scenarios when compared to its predecessors. The main features of 11ax can be summarized as,

- Simultaneous communication of multiple clients on the same spectrum
- A dense Access Point (AP) deployment without reducing the overall throughput.

First challenge is addressed by multiplexing the clients both in space and frequency, with Multi-User Multiple Input-Multiple Output (MU-MIMO) and Orthogonal Frequency-Division Multiple Access (OFDMA), respectively. The second challenge, which already exist in cellular networks, is handled by introducing the frequency reuse planning and Basic Service Set (BSS) Colouring technologies to the standard. Thanks to the BSS Colouring, any device can now distinguish the source of the signal-on-air. Therefore, 11ax allows interference up to a certain level, instead of running back-off procedures which reduces the overall throughput. Once the source of the interferer is identified (whether intra-cell or inter-cell) by its BSS Colour, multiple mechanisms can be used in order to enable a reliable link, thanks to the flexibility introduced by OFDMA and MU-MIMO [3].

From an active radar point of view, several studies exist in the literature that identify the impact of interferences. It is shown in [4] that interferences can yield ghost targets, ridges

or increased noise floor on range/Doppler maps (RDM). However, most of the active radars use different waveforms such as Frequency Modulated Continuous Wave (FMCW), instead of Orthogonal Frequency-Division Multiplexing (OFDM) modulation. In [5], the impact of interference between two active radars that use OFDM and FMCW waveforms is studied. It is concluded that an interfering OFDM waveform increases the noise floor of an FMCW radar. On the other hand, the impact of interference in the PR context becomes relevant when the PR is paired with an 11ax AP. The main reason is that for most of the scenarios considered by the standard committee, 11ax APs will be deployed with a high density. Even if there is frequency reuse planning, APs that share the same spectrum can be as close as 30 meters from each other [6]. Since the impact of interference between OFDM radars is not well addressed in the literature, the goal of this work is to address the possible degradations that can occur on RDMs. We limit the numerical analysis for a PR scenario where the SoO and interferer are OFDM signals, modulated to be compliant with the 11ax standard. However, the mathematical models that show the impact of interference are applicable for active OFDM radars as well.

This paper is structured as follows: In Section II, we briefly introduce the 11ax OFDM parameters which are relevant for the PR context. We also briefly discuss the deployment and interference scenarios considered by the standard committee. In Section III, we introduce the mathematical models for OFDM radar processing in the presence of an interferer. In Section IV, we numerically assess the radar performance by considering a PR that uses an 11ax AP as the source of SoO, while it is interfered by another 11ax AP. Finally, in Section V, the conclusion is drawn.

II. 802.11AX SIGNALS AND SCENARIOS

One of the new features of 11ax is to support simultaneous communications. To do so, OFDMA is used which splits the spectrum into Resource Units (RUs) to be allocated for different users. To improve the spectrum allocation flexibility of OFDMA, the total number of subcarriers is increased with a factor of 4 compared to the previous versions of the standard. Since the available bandwidths have not changed, the subcarrier spacing is reduced with a factor of 4; introducing longer OFDM symbols. Moreover, the maximum Cyclic Prefix (CP) duration is increased to support outdoor communications where the delay spread is larger compared to indoor environments. These parameters are summarized in Table I.

Standard	802.11ac	802.11ax
Carrier Frequency	5 GHz	2.4 and 5 GHz
Bandwidth	20, 40, 80 and 160 MHz	
FFT Size	64, 128, 256 and 512	256, 512, 1024 and 2048
Subcarrier Spacing	312.5 kHz	78.125 kHz
Symbol Duration	3.2 μ s	12.8 μ s
Cyclic Prefix	0.4 or 0.8 μ s	0.8, 1.6 or 3.2 μ s

TABLE I: OFDM parameter evolution.

Since densely deployed APs are considered, a new mechanism called BSS Colouring has been introduced to prevent network congestion. Legacy Wi-Fi devices sense the channel with the Carrier Sense Multiple Access-Collision Avoidance (CSMA-CA) mechanism, to ensure its availability before communicating. In the unlucky case of a collision between information bursts transmitted by two different devices, the bursts are retransmitted after a random delay, i.e. back-off procedure. Therefore, in the case of legacy Wi-Fi networks, it is reasonable to assume that successfully transmitted information bursts are not significantly corrupted by interference. On the other hand, the emerging 802.11ax standard targets a dense deployment of the Wi-Fi networks in crowded environments. Since the traditional CSMA-CA mechanism would incur too many back-off procedures, it has been updated to afford low-power interferences among cells sufficiently far away from each other (see BSS Colouring mechanism in [7]).

The new mechanisms of the 11ax standard (such as OFDMA and BSS Colouring) require some extensions on the preamble of every frame. Independent from the type of the transmission (whether it is Single-User or Multi-User), the preamble has common fields. The frame starts with the Legacy block which is used to estimate the start of the frame and correctly decode the rest of the preamble. HE-SIG-A field contains information on the parameters for the communication, as well as the BSS Colour. Since High Efficiency-Long Training Field (HE-LTF) is used to estimate the channel coefficients, it is located just before the data. The number of HE-LTF fields depends on the number of transmit antennas of the device, i.e. one HE-LTF signal per transmit antenna. The reader is referred to [7] for a description of the full preamble structure.

Since 11ax is designed to allow interference up to certain level, inter-cell interference could corrupt the PR. However, since the APs transmit even if there is low-power interference, it means that there are more opportunistic signals for the PR.

III. OFDM RADAR PROCESSING

A. Ideal Radar Processing

The transmitted signal is composed of M OFDM modulated symbols

$$s(t) = \sum_{m=0}^{M-1} \sum_{q=0}^{Q-1} c[q, m] \exp\left(j2\pi\left(\frac{q}{T_u}(t - mT)\right)\right) u(t - mT) \quad (1)$$

where $c[q, m]$ is the complex symbol of m th OFDM symbol mapped on the subcarrier q . The subcarrier spacing is defined as $\Delta_f = B/Q$, where B and Q are the signal bandwidth and

total number of subcarriers, respectively. Therefore, $T_u = Q/B$ and $T_g = K/B$ are defined as the useful signal and CP durations (where K is the number of samples in CP), respectively. We also define $k = T_g/T_u$ as the ratio between the two durations and $T = T_u + T_g$ as one OFDM symbol duration. The rectangular pulse-shaping function, $u(t)$ is defined as

$$u(t) = \begin{cases} 1, & 0 \leq t < T \\ 0, & \text{elsewhere} \end{cases}$$

A time-varying Channel Impulse Response (CIR) can be written as

$$h(\tau, t) = \sum_{p=1}^P \alpha_p \delta(\tau - \tau_p) \exp(j2\pi f_p t) \quad (2)$$

where P is the total number of multi-path components (MPCs). Assuming that the transmitter and the receiver are co-located, the propagation is two-way for the signal echoes. Therefore, α_p , $f_p (= 2v_p/\lambda)$ and $\tau_p (= 2d_p/c)$ are the complex amplitude, Doppler frequency and propagation delay per path, respectively. We assume that the time-variation of the complex amplitude is negligible while the speed of any target is assumed to be constant. For each path, v_p and d_p are defined as the radial speed and distance, respectively. In the context of PR, each MPC corresponds to the distance and velocity of a target. Therefore, estimation of the channel parameters in (2), is the objective of the radar receiver. The received signal at the antenna can be modelled as the convolution between (1) and (2) which yields

$$r(t) = \sum_{p=1}^P \sum_{m=0}^{M-1} \sum_{q=0}^{Q-1} \left(\alpha_p c[q, m] u(t - mT - \tau_p) \exp\left(j2\pi\left(\frac{q}{T_u}(t - mT - \tau_p)\right)\right) \exp(j2\pi f_p t) \right) + z(t) \quad (3)$$

where $z(t)$ represents the Additive White Gaussian Noise (AWGN) at the receiver of zero mean and variance σ_n^2 . If $T_g > \tau_p, \forall p$ (the CP duration is longer than the maximum path delay), the sampled received signal can be written as

$$r[n', m'] =: r(t = n'T_s + m'T), \quad n' = 0 \dots Q + K - 1 \quad (4)$$

where $T_s = 1/B$ is defined as the sampling interval. The sampled windowing function, i.e. $u(n'T_s + (m' - m)T - \tau_p)$, is equal to 1 only for $m' = m$. Then only the CP will contain the inter-block-interferences (IBI) since it serves as a buffer between OFDM symbols. The useful part of the OFDM symbols are not corrupted by the IBI, hence the received signal can be written in matrix form as follows

$$r[n, m] = \sum_{q=0}^{Q-1} c[q, m] \left(\exp(j2\pi(q + \varepsilon_p) \frac{n}{Q}) \cdot \sum_{p=1}^P \alpha_p \exp(j2\pi \frac{-q l_p}{Q}) \exp(j2\pi f_p m T) \right) + z[n, m] \quad (5)$$

where the columns contain the OFDM symbol samples and the rows contain only the useful parts of the OFDM symbols.

Here, $\varepsilon_p(=f_p/\Delta_f)$ is the normalized Doppler frequency with respect to the subcarrier spacing, and it indicates the Inter-Carrier-Interference (ICI) due to the Doppler shifts. However, since the Doppler frequency of relatively slow objects is much smaller than the subcarrier spacing, this term is negligible. $z[n, m]=z(t=nT_s+mT)$ is independently and identically distributed Gaussian variables, i.e. noise samples. Moreover, $l_p=\lfloor \tau_p/T_s \rfloor$ is the index of the range gate that is the closest to a given τ_p . For OFDM based radar processing, this term is linked to the range resolution, since range resolution is inversely proportional to the system bandwidth. Therefore, with a higher bandwidth (or a faster sampling interval), targets which are closer to each other can be resolved. It is also important to mention that multiple paths may fall into one tap. In such a case, l_p contains, forming a cluster on the given tap. The second line of (5) contains information about the channel coefficients. Assuming that the receiver has the knowledge of the transmitted symbols (in practice, HE-LTF of the preamble), once the DFT of (5) is computed, the estimated Channel Transfer Function (CTF) can be written as

$$\hat{H}[q, m] = \sum_{p=1}^P \alpha_p \exp(-j2\pi \frac{ql_p}{Q}) \exp(j2\pi f_p mT) + z[q, m] \quad (6)$$

Finally, the Inverse Discrete Fourier Transform (IDFT) of (6) yields M successive CIR estimates, i.e. the range profiles

$$\hat{h}[l, m] = \sum_{p=1}^P \alpha_p \delta[l - l_p] \exp(j2\pi f_p mT) + z[l, m] \quad (7)$$

Equation (7) is known as range/slow-time map, since the targets are separated with respect to their range, but not their speeds. If there are multiple targets clustered on one tap but with different speeds, a complex multi-sine is formed over a given tap, l , where each frequency component is associated with a Doppler frequency. To estimate the Doppler spectrum, the DFT on the second dimension of (7), i.e. DFT for each tap, can be computed which yields

$$\hat{h}[l, v] = \sum_{p=1}^P \alpha_p \delta[l - l_p] \cdot \sum_{m=0}^{M-1} \exp\left(j2\pi\left(m\left(v_p(1+k) - \frac{v}{M}\right)\right)\right) + z[l, v] \quad (8)$$

where $v_p=f_pT$. Notice that for a higher resolution on Doppler spectrum, M has to be increased. Since the DFT is applied on the useful part of the OFDM symbols, the effect of CP has to be withdrawn beforehand. If we consider a sufficiently long observation window, the DFT on (8) will yield a Kronecker Delta, such as

$$\hat{h}[l, v] = \sum_{p=1}^P \alpha_p \delta[l - l_p] \delta[v - v_p] + z[l, v] \quad (9)$$

Equation (9) is known as an RDM in the radar literature, which characterizes the channel in both delay-Doppler domains.

Notice that the range resolution is limited by the sampling frequency of the system, while the Doppler resolution is limited by the observation time. It is clear that any object in the channel will be represented as an element of this matrix, where the indices of the element depends on the distance and the speed of the corresponding object. The thermal noise acts like a noise floor on the RDM. Therefore, any signal echo with insufficient amount of amplitude will be hidden under the noise floor and it will not be detected.

B. Radar Processing with Interference

Similarly, an interfering signal can be modelled as

$$s_i(t) = \sum_{m=0}^{M-1} \sum_{q=0}^{Q-1} c_i[q, m] \exp\left(j2\pi \frac{q}{T_u}(t - mT)\right) u(t - mT) \quad (10)$$

where subscript i indicates that the parameter belongs to the interferer. We also assume that the interfering signal exists at least for the duration of MT . Since interfering signal propagates through a different channel, the received interfering signal can be written as

$$r_i(t) = \sum_{p_i=1}^{P_i} \sum_{m=0}^{M-1} \sum_{q=0}^{Q-1} \left(\alpha_{p_i} c_i[q, m] u\left(t - mT - \frac{\tau_{p_i}}{2}\right) \exp\left(j2\pi\left(\frac{q}{T_u}(t - mT - \frac{\tau_{p_i}}{2})\right)\right) \exp\left(j2\pi \frac{f_{p_i}}{2} t\right) \right) \quad (11)$$

where the channel parameters are also separated by the indices. Since the interfering signal propagates one-way, Doppler frequency and propagation delay are divided by 2. By following the same processing steps as before, the CTF, estimated at the PR, can be written as

$$\hat{H}_i[q, m] = \sum_{p_i=1}^{P_i} \alpha_{p_i} \frac{c_i[q, m]}{c[q, m]} \cdot \exp\left(j2\pi \frac{-ql_{p_i}}{2Q}\right) \exp\left(j2\pi \frac{f_{p_i}}{2} mT\right) \quad (12)$$

Here, it is clear that there are different cases that can occur. These cases depend on the interfering signal and SoO, and can be summarized as follows

- Interference signal is matched to the SoO ($c[q, m]=c_i[q, m], \forall q, m$);
 - *Case 1:* Transmitted complex symbols are equal, e.g. overlapping preambles.
- Interference signal is random ($c[q, m] \neq c_i[q, m], \forall q, m$);
 - *Case 2.1:* The interference is full band and the transmitted complex symbols are different, e.g. downlink signal of the interfering AP is overlapping with the preamble of the SoO.
 - *Case 2.2:* The interference is partial band, where only a subset of the subcarriers is loaded, e.g. uplink signal from the Client is interfering.

The estimated range/slow-time matrix (equivalent to (7) for the ideal case) varies depending on the scenario.

$$\hat{h}_i[l, m] = \sum_{p_i \in l} \exp(j2\pi f_{p_i} mT) \begin{cases} \delta[l - \frac{l_{p_i}}{2}], & \text{Case 1} \\ s_i^f[l - \frac{l_{p_i}}{2}, m], & \text{Case 2.1} \\ s_i^p[l - \frac{l_{p_i}}{2}, m], & \text{Case 2.2} \end{cases} \quad (13)$$

In the Case 1, the CTF will contain only the channel parameters since $c_i[q, m]/c[q, m]=1, \forall q, m$. Therefore, the CIR estimation yields ghost targets for every path which the interfering signal propagated through. Moreover, since PR receiver assumes two-way propagation for any signal echo, the ghost targets will appear at the half of their true distance. In the Case 2.1, the CTF estimate will contain random complex symbols, additional to the channel coefficients, since $c_i[q, m]/c[q, m] \neq 1, \forall q, m$. Notice that, in (7), the sum yields Q when $l=l_p$. For all values of $l \neq l_q$, the sum yields zero. However, in this case, every computation for the exponential will be disturbed by the additional symbols. Therefore, the terms that should lead to zero, will yield other complex values in time-domain. Hence, IDFT acts like an OFDM modulation, which yields a signal, $s_i^f[l, m]$, that spreads to all range bins that causes distortions. Moreover, since the data, i.e. complex symbols on the subcarriers, vary for the interfering signal the distortions will not be periodic over Doppler spectrum. Finally, the Case 2.2 is similar to the Case 2.1 with a slight difference: Since only a part of the band is occupied by the interferer, a few subcarriers of the CTF (in (6)) will be distorted. However, since every subcarrier contains information about every range bin, the distortion due to the partial band interference will spread to all range bins. But, the total amount of distortion on the RDM will be smaller than the full band interference case.

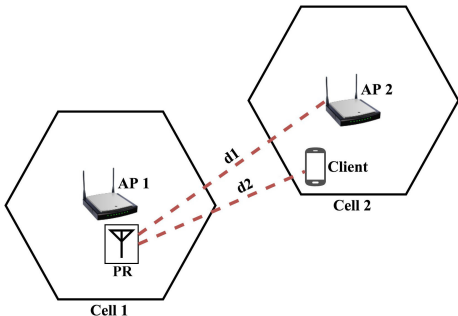


Fig. 1: Indoor Small BSS Hotspot scenario with two APs sharing the same spectrum. The signal from the Client is assumed to be an uplink signal.

IV. NUMERICAL RESULTS

In this section, the simulation results are discussed. The system parameters are summarized in Table II. The scenario considered in our simulations is given in Figure 1. The PR and AP1 are co-located and the source of the SoO is AP1. The two distances, d_1 (AP2-to-PR) and d_2 (Client-to-PR), are considered as variables between 30 and 150 meters. We assume that downlink signal of AP2 fully occupies the 80 MHz bandwidth, while uplink signal of the Client uses only a portion of the spectrum, i.e. different RU sizes. In order to find the limits of the PR performance in the presence of

an interferer, we consider a target at 20 meters distance with 4 dBsm Radar Cross Section (RCS), and a varying speed. Finally, PR only uses the HE-LTF part of the preamble for channel estimation as in [2]. Therefore, there is no reference signal reconstruction at the receiver, since the content of this field is known a priori.

Parameter	Value	Parameter	Value
Bandwidth	80 MHz	Gtx/Grx	2 dBi
Dwell Time	50 ms	Ltx/Lrx	3dB
#HE-LTF	4	Range Window	Tukey
Ptx	10 dBm	Doppler Window	Blackman

TABLE II: System parameters for the AP and the PR. The windows are applied to suppress the sidelobes on both delay and Doppler dimensions.

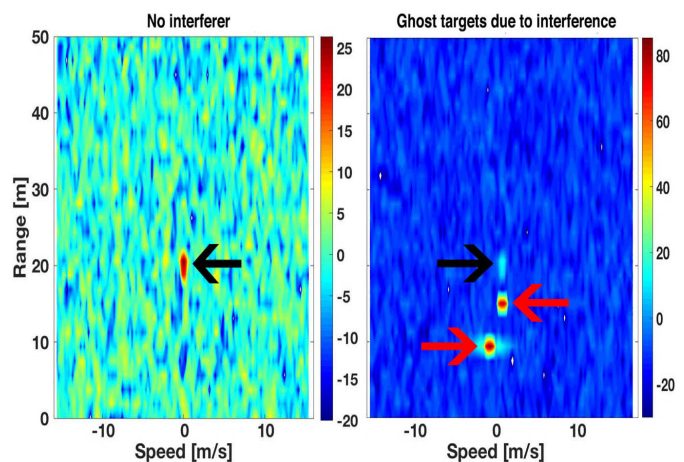


Fig. 2: RDM without interferer (left) and with matching interferer (right). Black and red arrows indicate the real target and the ghost targets, respectively.

In Figure 2, we show two simulation results. The ideal case (no interference) and when AP2 interferes on PR with time-aligned preambles (Case 1). The real distance and the speed of the AP2 and the Client are ($d_1=30\text{m}, 0\text{m/s}$) and ($d_2=20\text{m}, 2\text{m/s}$), respectively. However, the ghost targets appear at the half of the true distances and speeds, since the propagation of the interfering signals is only one-way. Moreover, due to the same reasoning, the path loss on the interfering signals is much smaller. Therefore, the ghost targets appear with stronger energy on the RDM compared to the real target.

In Figure 3, the RDM plots are shown for the Cases 2.1 and 2.2. In an OFDM-based range processing, all the subcarriers contain information about the distance of the targets. For the first two RDMs, only a subset of the subcarriers are distorted by the interference. Therefore, the RDM has relatively more contaminated ripples above the noise floor. However, when that subset is increased, the energy of the ripples increases to a level compared to the real target. In these two cases, additional ripples may cause a miss or false detection. In the last RDM plot, we show the case of having a full band interference. As expected, the interference causes the noise floor to increase significantly, since all subcarriers of the SoO are distorted by the interferer. In such a case, the targets beyond a certain range and below a certain RCS will not be detected.

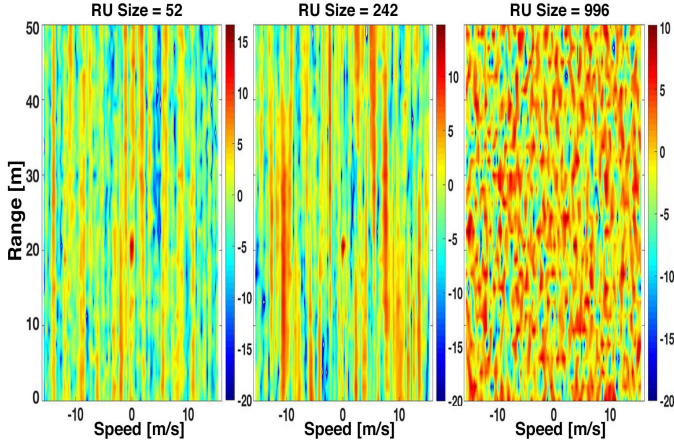


Fig. 3: Interference with different RU sizes: 52, 242 and 996 loaded subcarriers. First two RU sizes represent an uplink signal from a Client, and the latter one is a downlink signal from the interfering AP.

It is possible to find a safe distance between a PR and the interfering AP such that the considered real target can still be detected with a high probability of detection (P_d). To achieve this, Marcum's Q Function [8] is used which is defined as

$$Q(\gamma, \beta) = \int_{\beta}^{\infty} x \exp\left(-\frac{(x^2 - \gamma^2)}{2}\right) I_0(\gamma x) dx \quad (14)$$

where $I_0(\cdot)$ is the modified Bessel function of the first-kind and zero-order. Since this expression does not have a closed-form solution, numerical methods need to be used [9]. Here, β can be replaced by the normalized CFAR Threshold. On the other hand, γ is the received signal SNR. By fixing the probability of false alarm at a reasonable rate ($P_{fa}=10^{-6}$), and varying the distance and the RU size of the interferer, one can compute the P_d for each (γ, β) pair. In our simulations, one hundred realizations are used for a given RU size and distance (similar to the Monte-Carlo analysis), followed by the computation of P_d for each (γ, β) pair. The results of these computations are shown in Figure 4.

When the distance between the interferer and the PR is increased, the probability of detection increases since the path loss is inversely proportional to the propagation distance. Therefore, the noise-like effect of the interferer goes below the thermal noise of the PR. On the other hand, for a fixed distance, the RU size plays an important role as well. For brevity, only three different RU sizes are considered. The disturbances on the RDM, caused by the smaller RU sizes, have affordable impacts on the P_d , as it was shown in Figure 3. Therefore, the desired P_d can be achieved when the source of the interferer is beyond 40 meters. In other words, a Client of the interfering cell could be located as close as 40 meters, without causing significant degradations on the P_d . However, when the RU size increases, the required distance to obtain a reliable P_d also increases. In such a case, the distance between the interferer and the PR should be at least 80 meters for full-band interference.

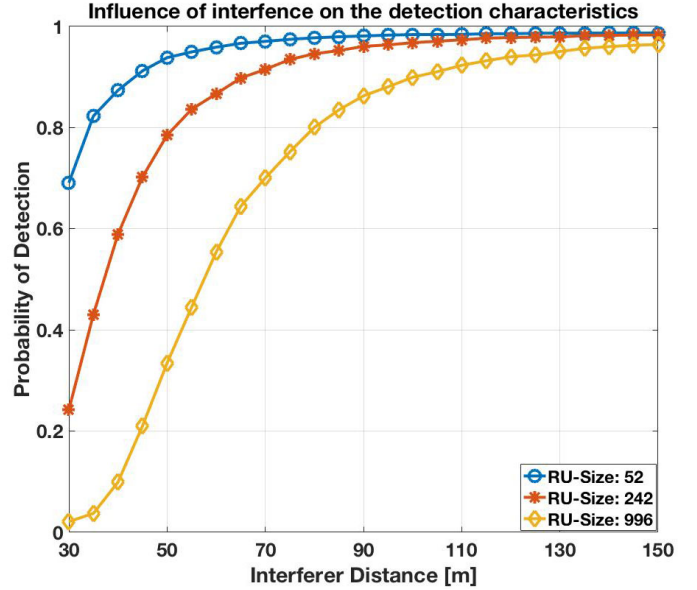


Fig. 4: Variation of probability of detection with respect to different interferer distances and RU sizes, while assuming that interferer and PR are in line-of-sight.

V. CONCLUSION

In this paper, we modelled the effects of OFDM radar interference in order to draw the limits to deploy a reliable PR. The generalized models and the PR specific numerical results obtained by the simulation chain show that the main degradations on an RDM are either ghost target(s) or an increased noise floor. The first type of degradation may/will cause false detections, while the latter one significantly reduces the probability of detection. The probability of detection, evaluated for different distances and RU sizes, diverges to an acceptable value when the interfering AP is 80 meters away.

REFERENCES

- [1] P802.11ax - IEEE Telecommunications and Information Exchange Between Systems Local and Metropolitan Area Networks – Specific Requirements Part 11: Wireless LAN Medium Access Control (MAC) and Physical Layer (PHY) Specifications Amendment Enhancements for High Efficiency WLAN
- [2] H. C. Yildirim, L. Storrer, M. Van Eeckhaute, C. Desset, J. Louveaux and F. Horlin, "Passive Radar based on 802.11ac Signals for Indoor Object Detection", IEEE EURAD 2019.
- [3] E. Khorov, A. Kiryanov, A. Lyakhov and G. Bianchi, "A Tutorial on IEEE 802.11ax High Efficiency WLANs", IEEE Communications Surveys & Tutorials Q1 2019
- [4] A. Bourdoux, K. Parashar and M. Bauduin, "Phenomenology of mutual interference of FMCW and PMCW automotive radars", 2017 IEEE Radar Conference (RadarConf)
- [5] C. Knill, J. Bechter and C. Waldschmidt, "Interference of Chirp Sequence Radars by OFDM Radars at 77 GHz", 2017 IEEE MTT-S International Conference on Microwaves for Intelligent Mobility (ICMIM)
- [6] IEEE 802.11ax High Efficiency Wireless LAN Task Group, "TGax Simulation Scenarios", <https://mentor.ieee.org/802.11/dcn/14/11-14-0980-16-00ax-simulation-scenarios.docx>, Last access: 12/06/19
- [7] Aruba Networks White Paper https://www.arubanetworks.com/assets/wp/WP_802.11AX.pdf, Last access: 29/05/19
- [8] Marcum, J. I. (1950) "Table of Q Functions". U.S. Air Force RAND Research Memorandum M-339. Santa Monica, CA, Jan. 1, 1950.
- [9] David A. Shnidman, "The Calculation of the Probability of Detection and the Generalized Marcum Q-Function", IEEE Transactions on Information Theory, Vol. 35, No.2, March 1989